Spatially Modulated Proton Minibeams Results in the Same Increase of Lifespan as a Uniform Target Dose Coverage in F98-Glioma-Bearing Rats

Authors: Lamirault, Charlotte, Brisebard, Elise, Patriarca, Annalisa, Juchaux, Marjorie, Crepin, Delphine, et al.

Source: Radiation Research, 194(6) : 715-723

Published By: Radiation Research Society

URL: https://doi.org/10.1667/RADE-19-00013.1

RADIATION RESEARCH **194**, 715–723 (2020)
0033-7587/20 $15.00

DOI: 10.1667/RADE-19-00013.1

Spatially Modulated Proton Minibeams Results in the Same Increase of Lifespan as a Uniform Target Dose Coverage in F98-Glioma-Bearing Rats

Charlotte Lamirault,[a,2] Elise Brisebard,[b,c,1,2] Annalisa Patriarca,[d] Marjorie Juchaux,[a] Delphine Crepin,[a] Dalila Labiod,[e] Frederic Pouzoulet,[e] Catherine Sebrie,[f] Laurene Jourdain,[f] Marine Le Dudal,[b,g] David Hardy,[b] Ludovic de Marzi,[d,h] Remi Dendale,[d] Gregory Jouvion[b,i] and Yolanda Prezado[h,3,4]

[a] *Laboratoire Imagerie et Modelisation pour la Neurobiologie et la Cancerologie, CNRS-Paris 7-Paris 11, Campus d'Orsay, France;* [b] *Department of Global Health, Experimental Neuropathology Unit, Institut Pasteur, 75015 Paris, France;* [c] *Laboratoire d'Histopathologie, VetAgro-Sup, Université de Lyon, Marcy l'Etoile, Lyon, France;* [d] *Radiation Oncology Department, Centre de Protonthérapie d'Orsay and* [e] *Experimental Radiotherapy Platform Institut Curie, University Paris Saclay, Orsay, France;* [f] *BioMaps, Université Paris-Saclay, CEA, CNRS, Inserm,Service Hospitalier Frédéric Joliot, 91401 Orsay, France;* [g] *Histologie, Embryologie et Anatomie Pathologique, Ecole Nationale Vétérinaire d'Alfort, Université Paris-Est, Maisons-Alfort, France;* [h] *Institut Curie, University Paris Saclay, PSL Research University, Inserm U 1021-CNRS UMR 3347, Orsay, France; and* [i] *Sorbonne Université, INSERM, Pathophysiology of Pediatric Genetic Diseases, Assistance Publique – Hôpitaux de Paris, Hôpital Armand-Trousseau, UF Génétique Moléculaire, Paris, France*

Lamirault, C., Brisebard, E., Patriarca, A., Juchaux, M., Crepin, D., Labiod, D., Pouzoulet, F., Sebrie, C., Jourdain, L., Le Dudal, M., Hardy, D., de Marzi, L., Dendale, R., Jouvion, G. and Prezado, Y. Spatially Modulated Proton Minibeams Results in the Same Increase of Lifespan as a Uniform Target Dose Coverage in F98-Glioma-Bearing Rats. *Radiat. Rev.* 194, 715–723 (2020).

Proton minibeam radiation therapy (pMBRT) is a new approach in proton radiotherapy, by which a significant increase in the therapeutic index has already been demonstrated in RG2 glioma-bearing rats. In the current study we investigated the response of other types of glioma (F98) and performed a comparative evaluation of tumor control effectiveness by pMBRT (with different levels of dose heterogeneity) versus conventional proton therapy. The results of our study showed an equivalent increase in the lifespan for all evaluated groups (conventional proton irradiation and pMBRT) and no significant differences in the histopathological analysis of the tumors or remaining brain tissue. The reduced long-term toxicity observed with pMBRT in previous evaluations at the same dose suggests a possible use of pMBRT to treat glioma with less side effects while ensuring the same tumor control achieved with standard proton therapy.

INTRODUCTION

There is an increasing body of evidence pointing toward the importance of the ''non-targeted'' effects in biological responses to radiation (*1–7*). In addition, there is an increasing number of published studies showing that the use of distinct temporal and spatial dose distributions can activate cell signaling (*7*) and vascular changes (*6*) as well as stromal and immunological modifications (*2, 3*) in the tumor and its microenvironment.

Along these lines, the use of highly modulated beams, such as in microbeam (MRT) (*8*) and minibeam (MBRT) radiation therapy (*9, 10*), appears to activate different biological mechanisms from those involved when direct damage by ionizing radiation occurs (*11–15*). Normal tissue sparing accompanied by tumor control has been demonstrated in small animal experiments using both MRT and MBRT (*15–26*). The need for complex requirements to achieve MRT conditions (very high-dose rates, low-kilovoltage energies (*27*) and challenging dosimetry) led to the exploration of minibeam radiation therapy with slightly larger (500–1,000 μm) beams. Being less vulnerable to beam smearing than MRT (*28*), the implementation of MBRT outside synchrotron sources to small animal irradiators is feasible (*29, 30*).

A recently reported approach is proton minibeam radiation therapy (pMBRT) (*31*). In pMBRT, a negligible dose is deposited in normal tissues after the Bragg peak (tumor position), further reducing secondary effects. In addition, multiple Coulomb scattering of protons allows a homogeneous dose distribution in the tumor with only one array of proton minibeams to be obtained if needed (*31*). pMBRT has been shown to notably reduce toxicity in skin of mice and rats (*32, 33*) and normal rat brains (*33*) compared to conventional broad beam irradiations.

Editor's note. The online version of this article (DOI: https://doi.org/10.1667/RADE-19-00013.1) contains supplementary information that is available to all authorized users.

[1] Scholar-in-training, Radiation Research Society.

[2] These authors contributed equally to this work.

[3] Previous address: Laboratoire Imagerie et Modelisation pour la Neurobiologie et la Cancerologie, CNRS-Paris 7-Paris 11, Campus d'Orsay, France.

[4] Address for correspondence: CNRS, Campus Universitaire, Bât. 440, 1er étage-15 Rue Georges Clemenceau, Orsay, Paris 91406 France; email: Yolanda.prezado@curie.fr.

In RG2-bearing rats, pMBRT was found to have an equivalent or superior effectiveness for tumor control compared to standard proton irradiation (*34, 35*). RG2 tumors are considered a good model to mimic human high-grade gliomas thanks to their aggressive and invasive nature and the induction of important vascular alterations (*36, 37*). A remarkable increase in mean survival was observed in the pMBRT groups, ranging from 20–67% depending on the level of dose heterogeneity in the target.

The purpose of this study was to extend our evaluations to other glioma cell lines with different characteristics (e.g., angiogenic capacity) which might affect the treatment outcome. We chose to evaluate the response of F98 tumor-bearing rats to pMBRT and broad beam irradiations. F98 is a widely used glioma cell line in oncology (*36*), classified as an anaplastic malignant tumor and displaying an infiltrative pattern of growth resembling human glioblastoma (GBM) (*36*). In contrast to RG2 tumors which are angiogenic, F98 glioma models use pre-existing blood vessels for their nutrient supply. In addition, F98 is mutant of p53, while RG model is wild-type of p53.

MATERIALS AND METHODS

All animal experiments were conducted in accordance with the animal welfare and ethical guidelines of our institutions. They were approved by the Ethics Committee of the Institut Curie and French Ministry of Research (permit no. 6361-201608101234488). Rats were anesthetized with isoflurane (2.5% in air) during irradiation and magnetic resonance imaging (MRI). At the end of the study, the rats were terminally anesthetized for brain fixation by the intracardiac perfusion of formalin zinc.

Tumor Cell Line and Tumor Implantation

The rat glioma cell line F98 (ATCC-2397TM; ATCC®, Gaithersburg, MD), which was transfected with the luciferase gene, was used. 10,000 F98-Luc cells were suspended in 5 μl DMEM and then injected intracranially into 344 male Fischer rats (Janvier Labs, Le Genest-Saint-Isle, France) using a Hamilton syringe through a burr hole in the right caudate nucleus (5 mm anterior to the ear-bars, i.e., at the bregma site, 3.0 mm lateral to the midline and 5.5 mm depth from the skull).

The presence of a tumor was verified by bioluminescence imaging (BLI) using an IVIS Spectrum (PerkinElmer® Inc., Waltham, MA). For the BLI procedure, the rats were injected intraperitoneally with a concentration of 150 mg/kg (P/N 122799) of D-luciferin (PerkinElmer) in 500 μl. Irradiations were performed six days after tumor implantation.

Irradiations and Dosimetry

The irradiations were performed at one of the horizontal beamlines (passive scattering) at the Orsay Proton Therapy Centre (ICPO; Orsay, France) with a proton beam energy of 100 MeV. The dose rate was 2 Gy/min at a 1-cm depth. To generate the minibeam, a multislit brass collimator was employed [400-μm-wide slits, 3,200-μm center-to-center distance (*38*)] and positioned 7 cm away from the rat skin. Gafchromic™ films were placed laterally on each side of the rat's head (beam entry and exit) and attached to the skin to allow for an assessment of the irradiation quality.

The same two configurations used in our previously published studies (*34, 35*) were employed. In the first experiment, four groups of animals (7 weeks old at the time of irradiation) were considered. Three of these groups were: 1. one control group (tumor-bearing rats, nonirradiated) (n = 5); 2. one group of tumor-bearing rats that received 25 Gy in one fraction at the Bragg peak in standard (seamless) proton irradiation (n = 9); and 3. another group that received pMBRT with a quasi-homogeneous dose distribution (25 Gy average) in the Bragg peak position (n = 9). Polymethyl methacrylate (PMMA), 49 mm thick, was placed in front of the rat's head to get the Bragg peak in the expected tumor position (*34*). This group is referred to as pMBRT_homog. The peak-to-valley dose ratio in the tumor was 1.20 ± 0.05. The peak, valley and mean dose at the Bragg peak position were 26 ± 2 Gy, 21.0 ± 1.0 Gy and 25 ± 2 Gy, respectively. The fourth group was comprised of tumor-bearing rats (n = 8) that received very heterogeneous dose distributions in pMBRT (58 ± 4 Gy peak dose, 9.5 ± 0.7 Gy valley dose, and 25 ± 2 Gy mean dose, at a depth of 1 cm). This group is referred to as pMBRT_heterog.25Gy.

In the second experiment, the same configuration as described elsewhere (*35*) was used. Two groups of animals were considered: 1. a control group (tumor-bearing rats, nonirradiated) (n = 5); and 2. a group of tumor-bearing rats (n = 9) of the same dose distribution as in experiment 1 (group 4) but with higher doses to assess whether an increase in survival could be expected (70 ± 5 Gy peak dose, 11.5 ± 0.8 Gy valley dose and 30 ± 2 Gy mean dose at a 1 cm depth). The tumor was irradiated in the plateau region. This group is referred to as pMBRT_heterog.30Gy.

More details on the dosimetry can be found in a study by Guardiola *et al*. (*39*). All the doses were delivered in one fraction to avoid any possible blurring inter-fraction of the minibeam pattern due to positioning errors.

Animal Follow-up

The animals were followed up for a maximum of six months. The clinical status of the animals was checked five times per week. Standard observations of animal well-being, namely weight gain, grooming, absence of vocalizations, irritability, and activity, were performed. Any rat showing classical adverse neurological signs related to tumor growth in the brain was humanely killed. These signs could be any of the following: loss of appetite and substantial weight loss (>10% loss of body weight in 24 h), periorbital hemorrhages, seizures or prostration.

The animals in the first experiment underwent an anatomical MRI study one month after irradiation. For each imaging session, a contrast agent (gadolinium) was administered by means of a catheter inserted into the tail vein. A 7-Tesla preclinical magnet (Bruker Avance Horizontal 7-T; Billerica, MA) equipped with a 35-mm-diameter ''bird-cage'' antenna was employed. Three series were acquired:

1. Morphological T2-weighted (T2W) images with a repetition time (TR) of 2,500 ms, an echo time (TE) of 33 ms, an echo spacing of 11 ms, rare factor 6, and a signal average of 2. In all, 21 slices were acquired.
2. T1-weighted (T1W) TurboRare sequences with a TR of 800 ms and TE of 6.05 m. A signal averaging of 2 was employed. A total of 21 slides were acquired. Three acquisitions were performed, one before and two (at 1.3 and 8 min) after the intravenous injection of a bolus of 100 μmol/kg Gd-DOTA (Guerbet SA, Villepinte, France).
3. T1 fast low-angle shot (FLASH) sequences with a TR and TE of 114.89 and 3.1 ms, respectively. A flip angle of 30° and a signal averaging of 4 were used. A total of nine slides were acquired in a total time of 1 min 28 s. Acquisitions were made just before, immediately after starting, and 6.30 min after intravenous injection of a bolus of 100 μmol/kg Gd-DOTA (Guerbet SA).

All experiments were acquired in axial orientation. The field of view was 35 mm × 35 mm, the in-plane resolution amounted to 0.137 mm × 0.137 mm, and the slice thickness and gap were 0.8 and 0.3 mm, respectively.

Histopathology and Immunohistochemistry

Animals from the first experiment, except for the pMBRT_heterog. 25Gy group, and animals from the second experiment were submitted to Institut Pasteur for histopathology and immunohistochemistry. Due to the sudden death of some rats, necropsy could not be carried out for all animals; 29 brains were available for histopathology and 26 tumors (histology is not a sensible method to detect microscopic focal lesion) were evaluated. See Supplementary Table S1 (https://doi.org/10.1667/RADE-19-00013.1.S1) for more details.

During necropsy, the brain was fixed by intracardiac perfusion of a fixative solution (formalin zinc). It was then removed and placed in the fixative before being embedded in paraffin. Several parasagittal sections of the right side of the brain (between 1 and 5), separated by 200 to 800 μm, were cut and stained in hematoxylin and eosin (H&E) to detect tumors. For rats that survived long-term (with no tumor assessed in the MRI), three sections separated by 400 μm each were analyzed.

Tumor size was measured using Zen software (Carl Zeiss AG, Oberkochen, Germany) on digitalized slides (whole-slide-scanning; AxioScan Z1; Carl Zeiss).

Once the tumor was assessed on H&E slides, four serial tissue sections (4 μm thick) were cut and used for immunohistochemistry (IHC) analysis to assess microglial morphology (anti-Iba-1 antibody, dilution: 1:500; Wako Chemicals, Richmond, VA) and the presence of T cells and T-cell subtypes [anti-CD3 antibody, 1:400 (Dako Inc., Carpinteria, CA); anti-CD4 antibody, 1:150 (Cell Signaling Technology® Inc., Danvers, MA); and anti-CD8 alpha antibody, 1:100 (Abcam®, Cambridge, MA)]. IHC staining was performed using a BOND RX Autostainer (Leica Biosystems, Nussloch, Germany) using the BOND Intense R Detection Kit (Leica Biosystems).

Microglial cell morphology is linked to their physiological state. Thus, neuroinflammation is characterized by ''reactive'' microglial cells displaying a larger cell body and thicker cell processes or little to no cell processes, with amoeboid form. They can also be grouped as clusters (microglial nodules) in the tissue. To evaluate neuroinflammation, a semi-quantitative method was used. Scores ranged from 0 (''resting'' microglia with thin processes) to 5 (hyperplasia of amoeboid microglial cells).

For T-cell infiltration, a semi-quantitative evaluation of CD3, CD4 and CD8 markers was performed, with the infiltration scored between 0 and 4 (0: none to minimal; 1: mild; 2: moderate; 3: marked; and 4: severe) for tumoral tissues, and between 0 and 2 (0: none; 1: representing less than 50% of the tumoral circumference; 2: representing more than 50% of the tumoral circumference) for peritumoral tissues. Histopathological analysis was carried out by two trained veterinary pathologists in a blind study.

Statistical Analysis

The median survival time after implantation was calculated, and Kaplan-Meier survival data were plotted versus time after tumor implantation. The survival curves were compared using the log-rank test between the irradiated group and controls (GraphPad Prism; La Jolla, CA).

For the histopathological and immunohistochemical data, due to the low number of animals in both control groups ($n = 5$), only a descriptive statistical analysis was applied. R software (http//www.R-project.org/) was used for the heatmap representation.

RESULTS

Survival

Concerning the MRI acquisitions performed one month postirradiation, all the animals except those with long-term survival exhibited large tumors. Figure 1 shows an example of an animal with a tumor and the other a long-term survival animal without one.

Figure 2 shows the survival curves of tumor-bearing rats. The curves corresponding to the irradiated animals are significantly statistically different from those of the nonirradiated controls ($P < 0.0001$ for experiment 1 and $P = 0.0019$ for experiment 2).

The survival curves are statistically equivalent for the groups receiving the same average dose (25 Gy), standard proton irradiation, pMBRT_homog and pMBRT_heterog.25 Gy, despite the highly heterogenous dose coverage in the latter group. One animal in the pMBRT_homog group survived for the entire duration of the study and was then censored.

The increase in lifespan (ILS) compared to the controls is equivalent in the standard proton irradiation (108 ± 17%), pMBRT_homog (74 ± 17%) and pMBRT_heterog.30Gy (106 ± 12%) groups. The ILS of the pMBRT_heterog.25Gy group (58 ± 10%) is significantly shorter and not included in the in-depth evaluations.

Histopathology and Immunohistochemistry

For histological examination, tumors of 26 rats were evaluated (16 from experiment 1; and 10 from experiment 2). No significant differences in cell morphology were observed between the groups and experiments. Intratumoral necrosis was common, significantly seen in 13/16 tumors in experiment 1 (81%) and 7/10 in experiment 2 (70%). No differences in the tumor cross-sectional area were observed between groups in the histology slides. Specifically, in experiment 1, these were: for controls, 10.0 ± 7.4 mm^2; for pMBRT_homog, 13.0 ± 8.6 mm^2; and for standard proton irradiation, 16.0 ± 11.9 mm^2. In experiment 2, these were: for controls, 12.0 ± 10.6 mm^2; and for pMBRT_heterog.30Gy, 17.0 ± 8.7 mm^2. These measurements correspond to the tumor size at the moment animals were sacrificed. Tumors were multifocal (except for one rat from experiment 2 in the pMBRT_heterog.30Gy group; the tumor was only observed in the meninges), including predominantly periventricular spaces (21/26 tumors, 81%), thalami (19/26 tumors, 73%), meninges (18/26 tumors, 69%) and, less frequently, hippocampi (5/26 tumors, 19%), cerebral cortices (5/26 tumors, 19%) and cerebella (4/26 tumors, 15%) (see Fig. 3). In the remaining ''normal'' brain parenchyma (around the tumors), we did not observe significant lesions (no necrosis or large foci of mineralization) except foci of ''reactive'' microglia with highly heterogeneous severity between the rats, even for those in the same groups. More details can be found in the Supplementary Table S1 (https://doi.org/10.1667/RADE-19-00013.1.S1).

The evaluation of microglial cell morphology using Iba-1 IHC did not reveal any clear difference between the groups. In experiment 1, the density of microglial cells infiltrating the tumors appeared slightly more important in the standard

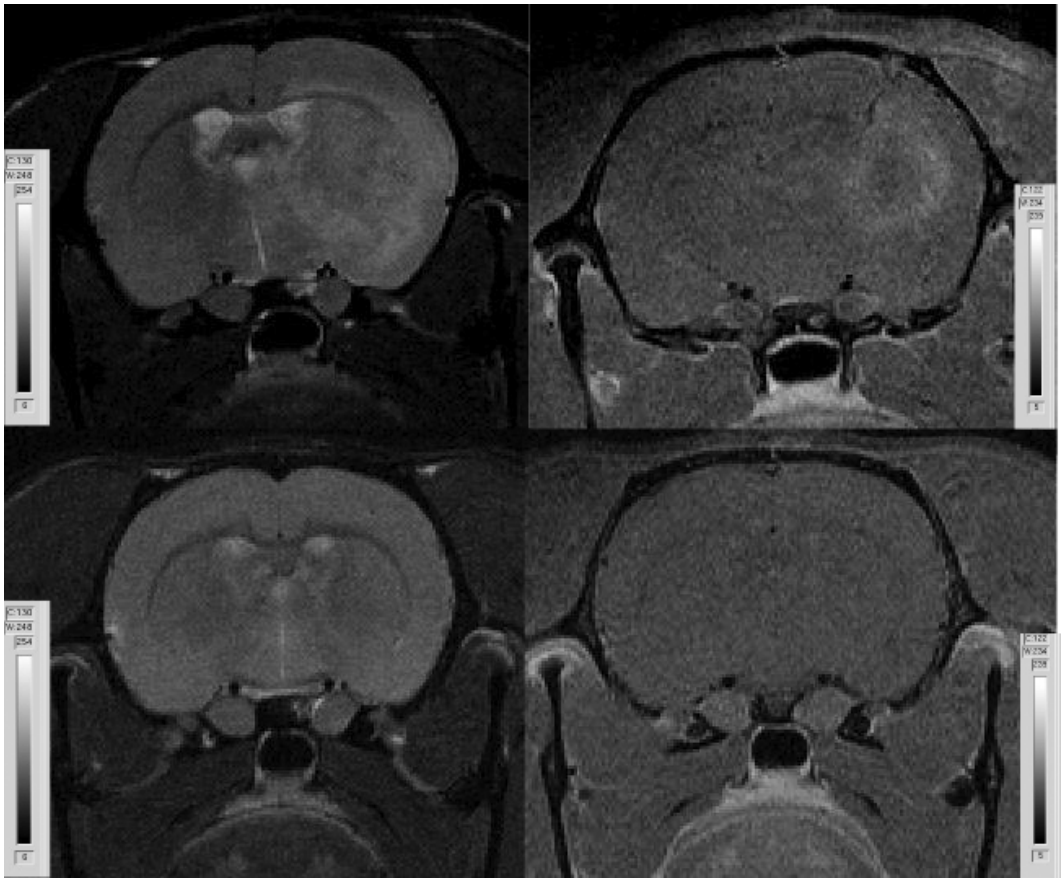

FIG. 1. MRI images of two animals included in experiment 1. The top row shows T2 (left side) and T1 RARE after contrast injection (right side) acquisitions with one of the animals showing a large tumor one month after irradiation. The bottom row shows the same sequences for a long-term survival animal.

proton irradiated group than in the pMBRT_homog group. Yet, because of an important variability, no significant differences could be found (see Fig. 3).

Tumoral and peritumoral T-cell infiltration was mild to moderate (Fig. 4). There was a wide individual variability in the two experiments. In experiment 1, no difference was seen for CD3, CD4 and CD8 expressions. In experiment 2, there appeared to be less intratumoral T cells in the pMBRT_heterog.30Gy group than in the control group.

DISCUSSION

Tumor dose conformation has significantly improved in the last decades owing to technological advancements such as image-guidance radiotherapy and particle therapy, among others. However, the treatment of some radioresistant tumors, tumors close to a sensitive structure (e.g., the central nervous system) and pediatric cancers, is still compromised due to the tolerance of normal tissues. This is especially critical in the case of brain tumors, such as GBM, which is the most common and most aggressive primary brain tumor in humans. Currently, the standard-of-care treatment for GBM patients is surgery followed by a combination of radiation and adjuvant chemotherapy with temozolomide (TMZ) (40). The median survival is still 14 months, largely due to GBM resistance to current radio- and chemotherapies (*41*). The benefit of proton therapy for GBM was evaluated in a phase II clinical trial (*42*) in which a total dose equivalent to 90 Gy was delivered. An increased overall survival (of 20 months) was achieved at the price of high rates of symptomatic necrosis necessitating neurosurgical intervention. Therefore, an effective treatment strategy could be to minimize normal tissue toxicity to further escalate the dose. Along this line, proton minibeam radiation therapy is an innovative approach which has already proven its ability in rats to reduce neurotoxicity with average doses of 25 Gy (58 Gy peak dose, plateau region) and 30 Gy (70 Gy peak dose, plateau region) in a single fraction (*33–35*). This contrasts with conventional proton irradiation where severe damage has been observed (*33–35*). In previously published work, we have shown that this increase of normal brain tolerance provided by pMBRT could be used to widen the therapeutic window for RG2 glioma-bearing rats (*34, 35*).

In this new study, we assessed the response of a different type of rat glioma, F98, to determine how different tumor features might affect treatment outcomes. The differences

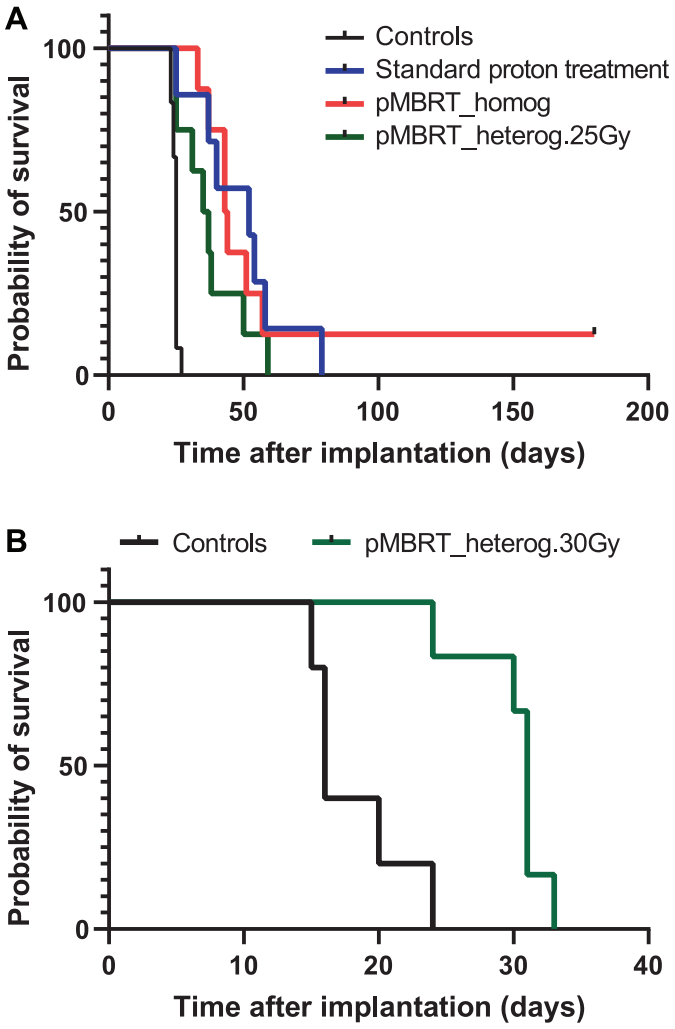

FIG. 2. Irradiation significantly increases the mean survival time of the treated animals with respect to the controls independent of the configuration. The survival curves of experiment 1 are shown on the left side. The curves of the irradiated groups [standard proton treatment (blue line), pMBRT with quasi_homog tumor dose coverage (red line) and pMBRT_heterog.25 Gy (green line)] are equivalent and statistically different from the control group ($P < 0.0001$). One animal in the pMBRT_homog group survived for the entire duration of the study and was then censored. The survival curves of experiment 2 are shown on the right side. pMBRT_heterog 30 Gy (green line) exhibits an increased lifespan compared to the controls.

could also provide some insights about the mechanisms of pMBRT.

A statistically significant increase in mean survival time was achieved in all irradiated series with respect to nonirradiated controls. The survival curves were equivalent in the three groups (standard_PT, pMBRT_homog, and pMBRT_heterog.25Gy), which received the same average dose (25 Gy) despite different dose distributions. However, the main limitation of our study is the lack of an individual treatment plan for each animal receiving irradiation, which would include an accurate delineation of the tumor volume based on an MRI performed on the day of the irradiation. This results in an increased uncertainty in the dose distributions delivered to the actual tumor volume and hinders our ability to establish a sound relationship between biological response and dosimetry parameters.

Our results appear to challenge the generally accepted assumption that the valley dose is the most relevant dosimetry parameter for tumor control in MRT. As of today, only a few studies have compared the biological effects of MRT against standard seamless irradiations (*15, 20, 43*). Most of those studies assessed the response of animals which received MRT with the valley dose equaling the dose delivered in standard irradiation (*15, 20*). The higher corresponding average doses in MRT with respect to standard irradiation in those studies might (partially) explain the higher tumor control rate in MRT. Systematic evaluations on the correlation between the different dosimetric parameters and biological response in SFRT are still needed to establish a sound method for dose prescription. Interestingly, the ILS is also equivalent to the standard_PT, pMBRT_homog, and pMBRT_heterog.30Gy groups. The fact that the same ILS could be obtained with a standard homogeneous dose distribution and highly heterogeneous dose coverage (pMBRT_heterog) seems to challenge the paradigms of classical radiotherapy and points at the participation of some non-targeted effects (*1–7*), such as immune system involvement, bystander effects, and/or other currently unknown mechanisms.

Concerning experiment 1 (quasi-homogeneous dose distributions), in contrast to RG2-bearing rats that had long-term survival rates of 2/9 and 5/9 in the standard proton irradiation and pMBRT_homog groups, respectively, only one long-term survival was achieved in the pMBRT series of F98 glioma-bearing rats. The different results obtained in the conventional irradiations of the two tumor types (see Fig. 5), indicate the different level of radiosensitivity of the two cell lines. F98 has been reported to be more radioresistant (*44*). However, while pMBRT_homog leads to a much larger proportion of long-term survivals than standard proton treatment for RG2-bearing rats, the response of the pMBRT group is equivalent to the broad beam treatment for F98 tumors. We could speculate that this could be linked to the fact that F98 is a mutant of p53. It has been suggested that the p53 pathway is involved in cell responses to bystander signals and that cells mutant to p53 are not able to respond to bystander signals (*13, 45*). Thus, cell signaling effects would be somehow reduced in F98 tumors. We could also hypothesize that pMBRT has a preferential effect to damage the newly formed (less mature) tumor vessels, of which RG2 tumors are more dependent, while F98 has a higher ability to hijack normal vasculature of the brain for its supply (*36*).

Regarding experiment 2 (highly heterogeneous dose distributions), while it holds true that no long-term survivals were seen in F98-bearing animals, the mean survival time was slightly longer than that of RG2-bearing animals. However, the differences are not pronounced enough to infer any conclusion. The results of this study are

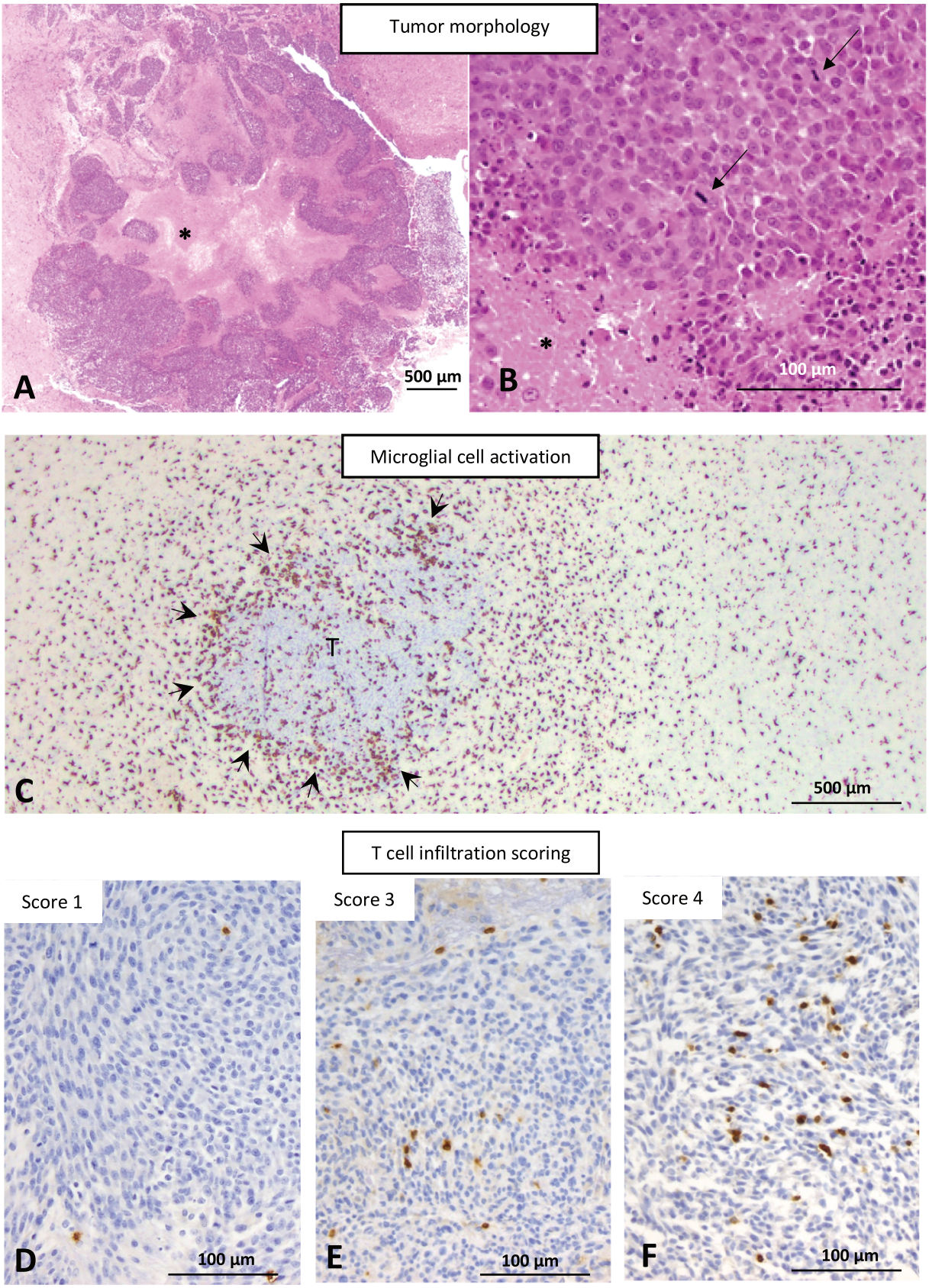

FIG. 3. Microscopic appearance of F98 rat glioma. Panel A: Representative microscopic aspect of tumors with central necrosis (*) in H&E. Panel B: Higher magnification showing neoplastic cells, with some mitotic figures (arrows) and necrosis (*) in H&E. Panel C: Ring of microglial cells (arrows) around the tumor (T), anti-Iba-1 IHC. Panels D–F: Intratumoral T-cell infiltration scoring, score 1 (panel D), score 3 (panel E) and score 4 (panel F), anti-CD3 IHC.

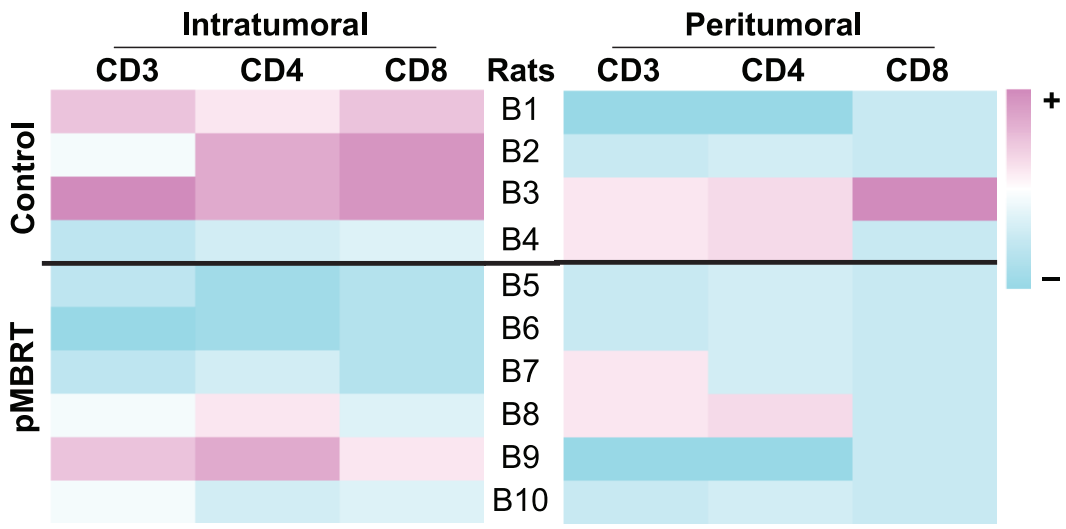

FIG. 4. Heatmap of T-cell infiltration in experiment 2. Distribution of the T-cell infiltrate scoring in the tumors and peritumoral brain tissue was obtained using R software for statistical analysis. Minimal infiltration is visualized in intense cyan, moderate infiltration in pale colors, and more severe infiltration in intense pink.

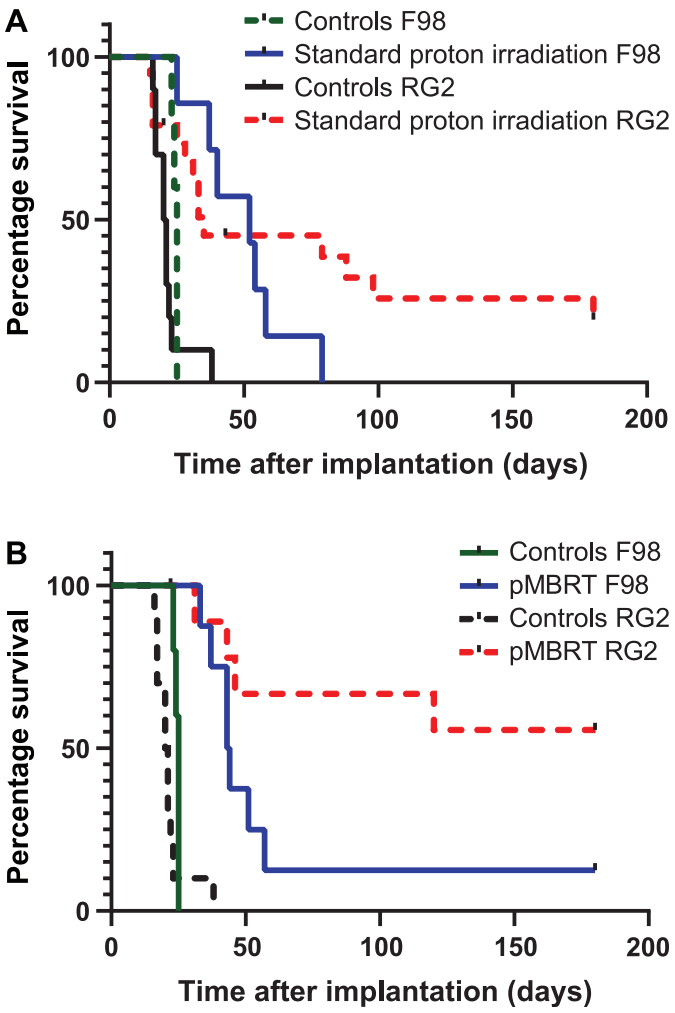

FIG. 5. Comparison of survival curves for RG2 and F98 tumor-bearing animals receiving standard broad beam irradiations (left) and pMBRT (right).

comparable to those of Deman *et al.* (*24*), who treated a series of F98-bearing rats with interlaced synchrotron MBRT at 54 Gy. They obtained an ILS of 113%, which is equivalent to our results at a lower dose and without the complexity required for interlaced MBRT.

Concerning the histo-immunohistochemical analysis, no significant differences among the analyzed groups in the two experiments were observed. This might be due to the fact that the animals were sacrificed when the end points associated with tumor growth were observed. This could explain the similarity in tumor cross-sectional areas and microglial and lymphocyte reactions. Additional short-term evaluations are needed to better characterize these effects. In addition, the optimization of irradiation parameters, such as beam spacing, doses, and the use of several entry ports, might further increase the therapeutic index.

CONCLUSIONS

This study showed that proton minibeam treatment increases the therapeutic index in F98 glioma-bearing animals. The same increase in lifespan was achieved in animals receiving standard proton treatment and pMBRT with different levels of dose heterogeneity in the target. No differences in microglial and lymphocyte infiltration were found among the groups. Future research may include a personalized treatment plan for each animal, short-term evaluations, further optimization in terms of beam widths, spacing, and doses as well as mechanistic evaluations.

SUPPLEMENTARY INFORMATION

Table S1. Histopathology and microglial activation data.

ACKNOWLEDGMENTS

This project has received funding from the European Research Council (ERC) under the European Union's Horizon 2020 Research and Innovation Programme (grant agreement no. 817908). In addition, this work was partially funded by the Agence National de la Recherche (grant no. ANR-17-ERC2-0010-001), SIRIC 2018–2022: INCa-DGOS-Inserm_12554 and EDF (Commission Scientifique du Conseil de Radioprotection).

Received: December 11, 2019; accepted: August 14, 2020; published online: September 29, 2020

REFERENCES

1. Baker HE, Paget JTE, Khan AA, Harrington AJ. The tumor microenvironment after radiotherapy: mechanisms of resistance and recurrence. Nat Rev Cancer 2015; 15:409–25.
2. Fromenti S and Demaria S. Systemic effects of local radiotherapy. Lancet Oncol 2009; 10:718–26.
3. Nesseler JP, Peiffert D, Vogin G, Nickers P. Cancer, radiotherapy and immune system. Cancer Radiother 2017; 21:307–15.
4. Prise KM, Sullivan JM. Radiation-induced bystander-signalling in cancer therapy. Nat Rev Cancer 2009; 9:351–60.
5. Rodel F, Frey B, Multhoff G, Gaipl U. Contribution of the immune system to bystander and non-targeted effects of ionizing radiation. Cancer Lett 2015; 356:105–13.
6. Park HJ, Griffin RJ, Hui S, Levitt SH, Song CW. Radiation-induced vascular damage in tumors: implications of vascular damage in ablative hypofractionated radiotherapy (SBRT and SRS). Radiat Res 2012; 177:311–27.
7. Schaue D, Kachikwu EL, McBride WC. Cytokines in radiobiological response: a review. Front Oncol 2012; 2:1–9.
8. Slatkin DN, Spanne P, Dilmanian FA, Gebbers JO, Laissue JA. Subacute neuropathological effects of microplanar beams of x-rays from a synchrotron wiggler. Proc Natl Acad Sci U S A 1995; 92:8783–7.
9. Dilmanian FA, Zhong Z, Bacarian T, Benveniste H, Romanelli P, Wang R, et al. Interlaced x-ray microplanar beams: a radiosurgery approach with clinical potential. Proc Natl Acad Sci U S A 2006; 103:9709–14.
10. Prezado Y, Renier M, Bravin A. A new method to generate minibeam patterns. J Synchrotron Radiat 2009; 16:582–6.
11. Bouchet A, Sakakini N, El Atifi M, Le Clec'h C, Brauer E, Moisan A, et al. Early gene expression analysis in 9L orthotopic tumor-bearing rats identifies immune modulation in molecular response to synchrotron microbeam radiation therapy, PLOS One 2013; 8:e81874.
12. Dilmanian FA, Qu Y, Feinendegen LE, Pena LA, Bacarian T, Henn FA, et al. Tissue-sparing effect of x-ray microplanar beams particularly in the CNS: Is a bystander effect involved? Exp Hematol 2007; 35:69–77
13. Fernandez-Palomo C, Brauer-Krisch E, Laissue J, Vukmirovic D, Blattmann H, Seymour C, et al. Use of synchrotron medical microbeam irradiation to investigate radiation-induced bystander and abscopal effects in vivo. Phys Med 2015; 31:584–95.
14. Bouchet A, Serduc R, Laissue JA, Djonov V. Effects of microbeam radiation therapy on normal and tumoral blood vessels. Phys Med 2015; 31:634–41.
15. Potez M, Fernandez-Palomo C, Bouchet A, Trappetti V, Donzelli M, Krisch M, et al., Synchrotron microbeam radiation therapy as a new approach for treatment of radio-resistant melanoma: Potential underlying mechanisms. Int J Radiat Oncol 2019; 105:1126–36.
16. Dilmanian F, Morris GM, Le Duc G, Huang X, Ren B, Bacarian T, et al. Response of avian embryonic brain to spatially segmented x-ray microbeams. Cell Mol Biol (Noisy-le-grand) 2001; 3:485–93.
17. Laissue A, Bartzsch S, Blattmann H, Brauer-Krisch E, Bravin A, Dallery D, et al. Response of the rat spinal cord to X-ray microbeam. Radiother Oncol 2013; 1:106–11.
18. Laissue A, Blattmann H, Di Michiel M, Slatkin DN, Lyubimova et al. The weanling piglet cerebellum: a surrogate for tolerance to MRT (microbeam radiation therapy) in pediatric neuro-oncology. Penetrating Radiation Systems and Applications III 2001; 4508:65–73.
19. Serduc R, van de Looij Y, Francony G, Verdonck O, van der Sanden B, Laissue J, et al. Characterization and quantification of cerebral edema induced by synchrotron x-ray microbeam radiation therapy. Phys Med Biol 2008; 53:1153–66.
20. Bouchet A, Brauer-Krisch E, Prezado Y, El Atifi M, Rogalev L, Le Clec'h C, et al. Better efficacy of synchrotron spatially microfractionated radiation therapy than uniform radiation therapy on glioma. Int J Radiat Oncol Biol Phys 2016; 95:1485–94.
21. Dilmanian FA, Button TM, Le Duc G, Zhong N, Pena LA, Smith JA, et al. Response of rat intracranial 9L gliosarcoma to microbeam radiation therapy. Neuro Oncol 2002; 4:26–38.
22. Dilmanian FA, Morris GM, Zhong N, Bacarian T, Hainfeld JF, Kalef-Ezra J, et al. Murine EMT-6 carcinoma: high therapeutic efficacy of microbeam radiation therapy. Radiat Res 2003; 159:632–41.
23. Laissue JA, Geiser G, Spanne PO, Dilmanian FA, Gebbers JO, Geiser M, et al. Neuropathology of ablation of rat gliosarcomas and contiguous brain tissues using a microplanar beam of synchrotron-wiggler-generated X rays. Int J Cancer 1998;78: 654–60.
24. Deman P, Vautrin M, Edouard M, Stupar V, Bobyk L, Farion R, et al. Monochromatic minibeams radiotherapy: From healthy tissue-sparing effect studies toward first experimental glioma bearing rats therapy. Int J Radiat Oncol Biol Phys 2012; 82:693–700.
25. Prezado Y, Deman P, Varlet P, Jouvion G, Gil S, Le Clec'H C, et al. Tolerance to dose escalation in minibeam radiation therapy applied to normal rat brain: Long-term clinical, radiological and histopathological analysis. Radiat Res 2015; 184:314–21.
26. Prezado Y, Sarun S, Gil S, Deman S, Bouchet A, Le Duc G. Increase of lifespan for glioma-bearing rats by using minibeam radiation therapy. J Synchrotron Radiat 2012; 19:60–5.
27. Prezado Y, Thengumpallil S, Renier M, Bravin A. X-ray energy optimization in minibeam radiation therapy. Med Phys 2009; 36:4897–902.
28. Manchado de Sola F, Vilches M, Prezado Y, Lallena A. Impact of cardiosynchronous brain pulsations on Monte Carlo calculated doses for synchrotron micro- and minibeam radiation therapy. Med Phys 2018; 45:3379–90.
29. Prezado Y, Dos Santos M, Gonzalez W, Jouvion G, Guardiola C, Heinrich S, et al. Transfer of minibeam radiation therapy into a cost-effective equipment for radiobiological studies: a proof of concept. Sci Rep 2017; 7:17297.
30. Bazyar S, Inscoe C, O'Brian E, Zhou O, Lee Y. Minibeam radiotherapy with small animal irradiators; in vitro and in vivo feasibility studies. Phys Med Biol 2017; 62:8924–42.
31. Prezado Y, Fois G. Proton minibeam radiation therapy: a proof of concept. Med Phys 2013; 40:031712.
32. Girst S, Greubel C, Reindl J, Siebenwirth C, Zlobinskaya O, Walsh DWM, et al. Proton minibeam radiation therapy reduces side effects in an in vivo mouse ear model. Int J Radiat Oncol Biol Phys 2016; 1: 234–41.
33. Prezado Y, Jouvion G, Hardy D, Patriarca A, Nauraye C, Bergs J, et al. Proton minibeam radiation therapy spares normal rat brain: Long-term clinical, radiological and histopathological analysis. Sci Rep 2017; 7:14403.
34. Prezado Y, Jouvion G, Patriarca A, Nauraye C, Guardiola C, Juchaux M et al. Proton minibeam radiation therapy widens the therapeutic index for high-grade gliomas. Scie Rep 2018; 8:1–10.
35. Prezado Y, Jouvion G, Guardiola C, Gonzalez W, Juchaux M, Bergs J, et al. Tumor control in RG2 glioma-bearing rats: A

comparison between proton minibeam therapy and standard proton therapy. Int J Radiat Oncol Biol Phys 2019; 104:266–71.

36. Barth RF, Kaur B. Rat brain tumor models in experimental neuro-oncology: the C6, 9L, T9, RG2, F98, BT4C, RT-2 and CNS-1 gliomas. J Neurooncol 2009; 94:299–312.

37. Doblas S, He T, Saunders D, Pearson J, Hoyle J, Smith N, et al. Glioma morphology and tumor-induced vascular alterations revealed in 7 rodent glioma models by in vivo magnetic resonance imaging and angiography. J Magn Reason Imaging 2010; 32:267–75.

38. Peucelle C, Nauraye C, Patriarca A, Hierso E, Fournier-Bidoz N, Martinez-Rovira I, et al. Proton minibeam radiation therapy: Experimental dosimetry evaluation. Med Phys 2015; 42:7108–13.

39. Guardiola C, De Marzi, Prezado Y. Verification of Monte Carlo dose calculation engine in proton minibeam radiotherapy in a passive scattering beamline for preclinical trials. Br J Radiol 2020; 93:20190578.

40. Furnari FB, Fenton T, Bachoo RM, Mukasa A, Stommel JM, Stegh A, et al. Malignant astrocytic glioma: genetics, biology, and paths to treatment. Genes Dev 2007; 21:2683–710.

41. Stupp R, Mason WP, van den Bent MJ, Weller M, Fisher B, Taphoorn MJB, et al. Radiotherapy plus concomitant and adjuvant temozolomide for glioblastoma. N Engl J Med 2005; 352:987–96.

42. Fitzek MM, Thornton AF, Rabinov JD, Lev MH, Pardo FS, Munzenrider JE, et al. Accelerated fractionated proton/photon irradiation to 90 cobalt gray equivalent for glioblastoma multiforme: Results of a phase II prospective trial. J Neurosurg 1999; 91:251–60.

43. Rivera JN, Kierski TM, Kasoji SK, Abrantes AS, Dayton PA, Chang SX. Conventional dose rate spatially-fractionated radiation therapy (SFRT) treatment response and its association with dosimetric parameters–A preclinical study in a Fischer 344 rat mode. PLOS One 2020; 15:e0229053.

44. Knedlitschek G, Anderer V, Weilbezahn KF, Dortinger H. Radioresistance of rat glioma cell lines cultured as multicellular spheroids. Correlation with electrical cell-to-cell-coupling. Strahlenther Onkol 1990; 166:164–7.

45. Mothersill C, Bristow RG, Harding SM, Smith RW, Mersov A, Seymour CB. A role for p53 in the response of bystander cells to receipt of medium borne signals from irradiated cells. Int J Radiat Biol 2011; 87:1120–5.